Pyrolysis Dynamics of Biomass Residues in Hot-Stage

Ivan Bergier,[a,*] Claudia M. B. F. Maia,[b] Marcela Guiotoku,[b] Paulo Paiva,[c] Ana Paula Silva,[a] and Etelvino H. Novotny [d]

Original data for mass, element, and methane dynamics under controlled pyrolysis are presented for several biomass feedstocks. The experimental system consisted of an environmental (low-vacuum) scanning electron microscopy (ESEM) with a hot-stage and energy-dispersive X-ray spectroscopy (EDS) detector. A tunable diode laser (TDL) was coupled to the ESEM vacuum pump to measure the methane partial pressure in the exhaust gases. Thermogravimetric analysis and differential thermal analysis (TG/DTA) in a N_2 atmosphere was also carried out to assess the thermal properties of each biomass. It was found that biochars were depleted or enriched in specific elements, with distinct methane formation change. Results depended on the nature of the biomass, in particular the relative proportion of lignocellulosic materials, complex organic compounds, and ash. As final temperature was increased, N generally decreased by 30 to 100%, C increased by 20 to 50% for biomass rich in lignocellulose, and P, Mg, and Ca increased for ash-rich biomass. Methane formation also allows discriminating structural composition, providing fingerprints of each biomass. Biomass with low ashes and high lignin contents peaks CH_4 production at 330 and 460 °C, whereas those biomasses with high ashes and low lignin peaks CH_4 production at 330 and/or 400 °C.

Keywords: Biochar; Agriculture; Residues; Manure; Soil fertilizer

Contact information: a: Biomass Conversion Lab, Embrapa, Corumbá, MS, Brazil; b: Soil Organic Matter/Biochar Lab, Embrapa, Curitiba, PR, Brazil; c: Soil Science/Biochar Lab, Embrapa Macapá, AP, Brazil; d: Soil Science/Biochar Lab, Embrapa, Rio de Janeiro, RJ, Brazil;
** Corresponding author: ivan.bergier@embrapa.br*

INTRODUCTION

In spite of the fact that the consequences of adding biochar to soils are still not fully understood (Spokas *et al.* 2012; Gurwick *et al.* 2013), this soil amender is expected to improve the productivity and environmental quality of agroecosystems similar to Amazonian Dark Earths (Novotny *et al.* 2009). Research has demonstrated that biochars play a significant role in mitigating soil greenhouse gas emissions (Case *et al*. 2012; Zhang *et al.* 2013; Nelissen *et al.* 2014), while others studies show the opposite (Troy *et al.* 2013) or neutral effects (Mukome and Parik 2013; Suddick and Six 2013). Biochar ash content, pyrolysis conditions, and C/N ratios seem to be key factors influencing N_2O emissions, while a direct correlation has been found between biochar application rate and N_2O emission mitigation (Liu *et al*. 2012; Cayuela *et al.* 2014). The ability of environmentally sound biochar to sequester carbon in soils depends on the characteristics of the receiving soil, as well as the structure and composition of the biochar (Lehmann *et al.* 2011; Yoo and Kang 2012). Biochars, in comparison to composts, tend to sequester C, yet a combination of both might be desirable for sustaining long-term fertility of soils (Bolan *et al.* 2012).

Appropriate combinations of feedstock and pyrolysis temperature are required to develop 'tailored' biochar for specific environmental/agricultural applications (Enders *et al.* 2012; Zhao *et al.* 2013). Biochars contain a range of nutrient forms with different release rates, which explains their variable effects on soil fertility with soil and crop type, and over time (Mukherjee and Zimmerman 2013). However, it has been shown that the mineral contents of biochar can play a significant role in agronomic responses, even for fertile soils (Rajkovich *et al.* 2012). Hence, the most effective approach for predicting agronomic performance of biochars is to identify the major limiting factors of a particular soil-crop-climate system and to apply tailored biochars to address growth constraints according to a library of characterization data (Lehmann *et al.* 2011; Enders *et al.* 2012). Determination of the element distribution in biochars from various feedstocks obtained at several temperatures is therefore crucial, particularly for scarcely studied biomasses with the potential to offer specificities to biochars.

Under this perspective, we present new data and an original method of analysis to investigate some pyrolysis properties of potential feedstocks for biochar production. The method relies on the environmental (pressure-variable) scanning electron microscopy (ESEM) described in Bergier *et al.* (2013). In brief, low-vacuum ESEM (water vapor atmosphere at 130 kPa maximum pressure), together with a hot-stage, allows the heating of a small biomass sample from room temperature to 1000 °C at controlled rates of temperature increases. Exhausted gases at the vacuum pump can be monitored during the ESEM low-vacuum pyrolysis, and the charred biomass can be exposed to EDS X-ray for elemental semi-quantitative analysis in SEM or ESEM mode (Bergier *et al.* 2013).

EXPERIMENTAL

Sources of Biomass Wastes

The feedstock biomasses considered in this study are the casing shells of the Brazil nut (*Bertholletia excels*) (Maia 2013; Paiva *et al.* 2013), Candeia wood tree (*Eremanthus erythropappus*) (Lima and Maia 2011; Maia 2013), floating macrophyte mats (several species, predominantly *Eichhornia* sp. (Castro *et al.* 2010), the solid phase of biodigested pig manure (Bergier *et al.* 2013), and coconut fiber (*Cocos nucifera*) (Maia 2013). Biomass samples were gathered by Embrapa Research Offices in the Amazonia, Pantanal, and Cerrado biomes in Brazil.

Samples of the casing fruit of *B. excels*, locally known as "ouriço" (Paiva *et al.* 2013), were analyzed separately for the fruit endocarp and epicarp. The residue samples of *E. erythropappus* were obtained from the extraction of α-bisabolol oil used for cosmetic and pharmaceutical purposes. This tree is usually found in mountain grasslands of Bahia, Minas Gerais, Rio de Janeiro, and São Paulo States in Brazil. Coconut production in Brazil is common, particularly in the Brazilian Northeast states. The obtained samples of coconut fiber (coir) are usually employed in potting compost/soil or as raw material for manufacturing ropes, mats, sacks, and other natural materials. Aquatic plant samples were obtained in the Pantanal wetland in the Mato Grosso do Sul State. Water hyacinth (*Eichhornia* sp.) and *Salvinia auriculata* are the predominant species in free-floating mats in the Paraguay River (Castro *et al.* 2010). Those species are regularly found in the Pantanal and in the Amazon River Basin. They have hastily spread around the world as invasive species, with severe impacts to wetlands and other freshwater ecosystems (Malik 2007). Samples of aquatic plants were analyzed individually in living (known as "camalote" in

Pantanal and "matupá" in Amazonia) and dead or semi-decomposed (known as "batume" in Pantanal) aquatic plant tissues.

The data used in this study for the solid phase of the bio-digested swine manure were obtained from Bergier *et al.* (2013), except for the pyrolytic methane formation experiment, in which new samples were used. Proximate analysis of ash, volatile matter, fixed carbon, lignin, and holocellulose contents were also obtained for the studied biomass samples.

EM-ESEM/EDS Design

Pyrolysis of biomass samples of approximately 5-mg wrapped in aluminum foil was carried out within the low-vacuum (water vapor atmosphere @ 130 kPa) chamber of an environmental (pressure-variable) scanning electron microscope (ESEM) FEI Quanta 250 (Eindhoven, Netherlands) equipped with an EDS ApolloX Ametek Edax (New Jersey, USA). The hot-stage is useful for thermodynamics experiments, including pyrolysis. The methodological procedures are described in Bergier *et al.* (2013). In short, four biomass samples (except for the digested swine manure, whose data were taken from Bergier *et al.* (2013)) for each feedstock was independently submitted to low-vacuum pyrolysis at 300, 500, 700, and 900 °C, with an increase rate of 20 °C/min. Each low-vacuum pyrolysis was conducted without activating the microscope electron beam (no image data). Therefore, the water vapor in the low-vacuum chamber was stable, *i.e.*, without ionized reactive hydrogen or oxygen and an almost O_2-free atmosphere. Alternatively, the aluminum foil did not prevent gaseous exchanges of the sample with the chamber environment. Some steam may react with the sample whereas the exhausted gases from thermal decomposition can be normally monitored at the vacuum pump, as further shown in results.

After returning to ambient temperature, the chamber was opened and the sample was recovered and weighed (the aluminum foil was previously weighed separately). The charred biomass package was subsequently opened and reinserted in the stage for EDS elemental semiquantitative analyses in SEM mode.

Mass changes following low-vacuum pyrolysis were roughly determined by discounting the weight of the sample package (aluminum foil) before and after each low-vacuum pyrolysis run (Bergier *et al.* 2013). The semi-quantitative EDS data assembles the median values of seven X-ray energy spectra per biomass type, and per pyrolysis temperature, including the original feedstock.

The EDS data were analyzed by the nonparametric statistic Kruskal-Wallis (K-W). The statistical significances of the differences in the median ± interquartile range of the element contents (wt.%) for the original biomass and the four final pyrolysis temperatures (degrees of freedoms, df = 4) were evaluated. In addition, for those changes that were statistically significant ($p < 0.10$), useful information of the semi-quantitative EDS data on the enrichment or depletion of elements in the biochar particles was obtained through graphical plots considering the relative change of each element as a function of the element content in the original feedstock (Table 1) and final pyrolysis temperature.

Thermal Mass Loss and Methane Formation

Thermal mass loss analyses under N_2 atmosphere were conducted on a Shimadzu (Kyoto, Japan) Thermogravimetric (DTG-60H) and Differential Thermal Analyzer (DTA-50). Biomass samples of approximately 5 mg were submitted to a heating rate of 10 °C/min from room temperature to 600 °C under a N_2 atmosphere at 20 mL/min. The rate of mass change $\Delta m/\Delta t$, where Δm is the infinitesimal mass change and Δt is the infinitesimal time

interval, was estimated by calculating the local first derivative of the obtained curves for each TG run.

The rates of methane (CH_4) formation for each feedstock were also assessed according to the increment in the hot-stage temperature in ESEM mode. A tunable diode laser (TDL, Ultraportable Greenhouse Gas Analyzer, Los Gatos Research Inc., California, USA) was adapted to the ESEM vacuum pump for the continuous measurement of CH_4 partial pressures in the exhaust gas at a frequency of 0.2 Hz. The adaptation of a silicone rubber stopper with two tubes (sampling and venting) enclosed a finite sized volume of approximately 4.7 mL at the vacuum pump outlet. The setup allowed the conversion of partial pressure (ppm or µmol/mol) into concentration (µM), assuming an ideal gas with $PV = nRT$. The time evolution of the methane concentration rate (µM/s) from room temperature to 1000 °C at 20 °C/min was estimated by calculating the local first derivative $\Delta C/\Delta t$, where ΔC is the infinitesimal concentration change of the obtained curve for each ESEM pyrolysis run.

RESULTS AND DISCUSSION

Biochar Yield in ESEM Hot-stage

For illustrative purposes, Fig. 1 shows EDS points measured in the surface of biochar particles produced in the hot-stage in ESEM at a final pyrolysis temperature of 700 °C.

The final pyrolysis temperature is particularly important for tailoring recalcitrant biochars (Uchimiya *et al.* 2013; Zhao *et al.* 2013). Generally, final pyrolysis temperatures above 400 °C produce recalcitrant and good-quality biochars (Cantrell *et al.* 2012; Enders *et al.* 2012; Uchimiya *et al.* 2013). However, pyrolysis above 800 °C (and under steam due to presence of some water vapor in the chamber) leads to biomass gasification and significant mass losses (Spokas *et al.* 2012). Biochar yield estimates for each feedstock biomass are shown in Fig. 2. The greatest biochar yield was obtained for the endocarp casing at 300 °C, while the lowest values were obtained for dead aquatic mats. Candeia tree feedstock presented the highest biochar production for temperatures between 300 and 700 °C.

Overall, a consistent increase or decrease in biochar yield as a function of the final temperature was not identified, which can be attributed to the low-vacuum mode or to methodological issues. Altogether, the low-vacuum chamber and the tiny sample sizes may have reduced the overall accuracy of weight measurements after ESEM pyrolysis. The mass weight measurements were made in a high-precision balance, although the amount of biomass employed in the experiment might be relevant for achieving better results in biochar yield, as those obtained in Bergier *et al.* (2013) for biomass around 10 to 20 mg. However, it is necessary to consider a limitation trade-off because higher initial biomass increases condensable volatiles in the microscope vacuum system, hence greater and more expensive will be the associated maintenance. Therefore, additional experiments are needed to clarify biochar yields under ESEM conditions. Nevertheless, biochar yield is ancillary data, as the main scope of the present study was to produce small amounts of charred biomass at various final temperatures to assess methane production and the relative change in elemental distribution by investigating semi-quantitative EDS data.

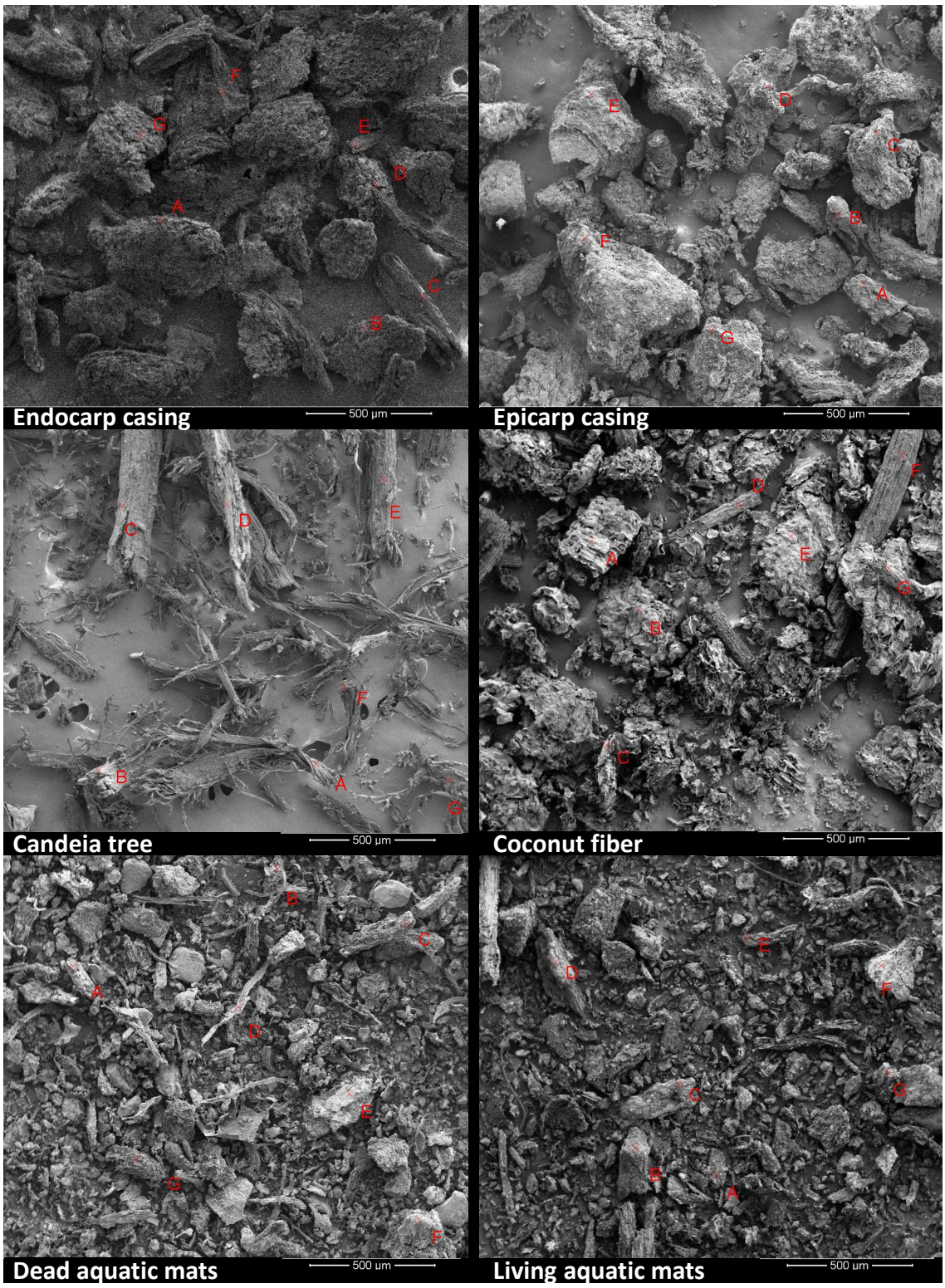

Fig. 1. Scanning electron microscopy (SEM) images of biochar particles produced at a final temperature of 700 °C. Letters A to G in each image indicate seven points of sample surface measurements by X-ray energy dispersive analysis (EDS).

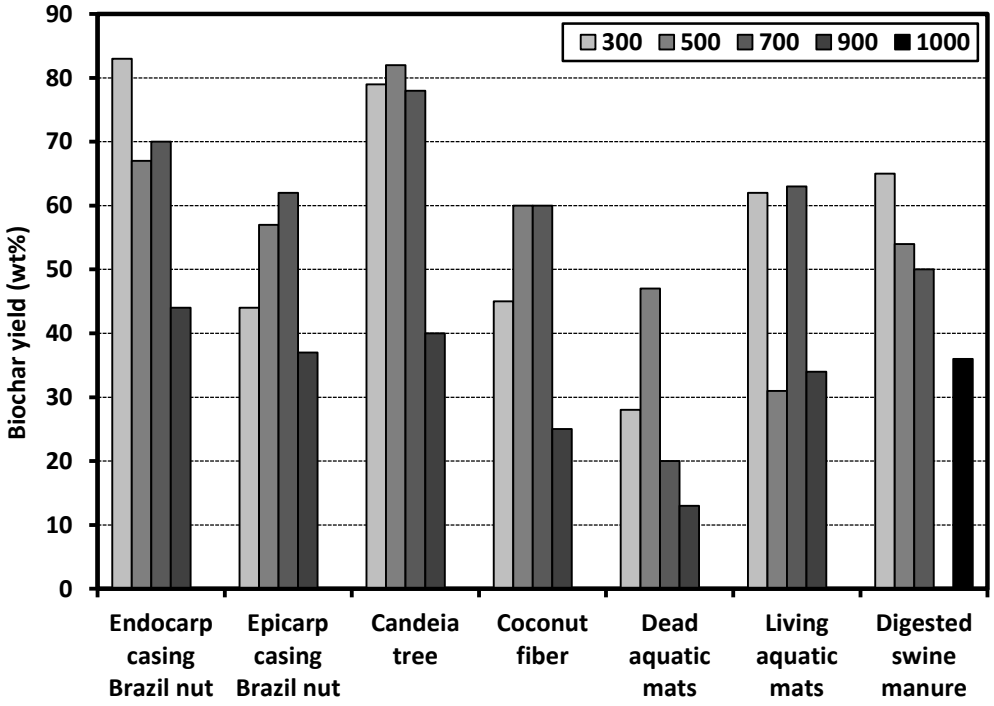

Fig. 2. Biochar yields by biomass and final pyrolysis temperatures

Semi-Quantitative SEM/EDS Data

The semi-quantitative EDS data for each biomass are shown in Table 1 as median values. For ultimate analysis, refer to data available in Maia (2013). There is a large abundance of mineral elements for digested swine manure, living aquatic mats, and epicarp casings of the Brazil nut. The solid phase of the swine digestate contains anaerobically biodegraded manure, urine, pig hair, and feed ration residues. Living aquatic plants are well-known for water purification by filtering dissolved solutes (Malik 2007). The epicarp casing is rich in K and Ca, whereas the endocarp casing essentially contains C, N, and O. An abundance of C, N, and O was also found for the Candeia tree, coconut fiber, and dead aquatic mats, but the latter also had a noticeable Si fraction (Table 1).

Table 1. Major Element Content (Dry Weight, wt.%) of Feedstocks Determined by Semi-Quantitative EDS Analysis (Median EDS Data Points, n = 7)

	C	N	O	Mg	Si	P	K	Ca
	wt.%							
Brazil nut endocarp casing	57.33	3.33	33.88	0.45	0.37	0.31	1.09	0.60
Brazil nut epicarp casing	53.09	4.83	35.08	0.56	0.24	0.25	2.72	0.21
Candeia tree	66.17	0.89	25.53	0.28	0.18	0.19	0.38	0.39
Coconut fiber	60.95	2.82	32.89	0.33	0.30	0.25	0.76	0.67
Dead aquatic mats	55.25	4.37	31.62	0.29	3.82	0.11	0.18	0.40
Living aquatic mats	35.83	1.62	20.66	0.57	7.83	0.80	9.74	3.65
Digested swine manure	40.10	5.44	30.45	3.29	3.29	1.02	1.44	5.11

For the original feedstock, the richest C content was found in the Candeia tree (66.2%), followed by coconut fiber (60.9%). The highest N content was found in the digested swine manure (5.4%), followed by the epicarp casing of the Brazil nut (4.8%) and dead aquatic mats (4.4%). The O content ranged from 25.5% to 35% in all feedstocks. Digested swine manure showed the greatest Mg (3.3%), P (1%), and Ca (5.1%) contents (Table 1). The biomass with the highest K content was the living aquatic mats (9.7%), followed by the epicarp casing of the Brazil nut (2.7%).

The K-W statistics (p values) to assess temperature effects on semi-quantitative EDS data are shown in Table 2. Statistical significances ($\alpha = 0.10$) were verified for C, N, and O of all feedstocks, excluding C for living aquatic plants and O for digested swine manure. Significant changes to Mg were found for the epicarp casing, living aquatic mats, and digested swine manure. Swine manure and both dead and living aquatic mats showed significant changes relative to Si. Significant changes in P occurred, particularly for the epicarp casing biomass and the digested swine manure, whereas K and Ca were significantly different for the endocarp/epicarp Brazil nut, coconut fiber, and digested swine manure.

Table 2. Kruskal-Wallis *p*-Values

	C	N	O	Mg	Si	P	K	Ca
Brazil nut endocarp casing	0.000	0.000	0.000	ns	ns	ns	0.000	0.004
Brazil nut epicarp casing	0.002	0.000	0.004	0.000	ns	0.004	0.000	0.000
Candeia tree	0.000	0.002	0.000	ns	ns	ns	ns	ns
Coconut fiber	0.061	0.007	0.000	ns	0.030	ns	0.000	0.009
Dead aquatic mats	0.002	0.022	0.048	ns	0.003	ns	ns	ns
Living aquatic mats	ns	0.008	0.009	0.010	ns	ns	ns	0.025
Digested swine manure[a]	0.005	0.000	ns	0.060	0.060	0.001	0.046	0.045
[a] (Bergier *et al.* 2013) and Table 1.								

*Non-significant *p*-values, assuming a chi-squared distribution with df = 4 and $p > 0.10$, are represented by "ns"

Considering only the significant results of the nonparametric statistical analysis (Table 2), the graph plots in Fig. 3 allow for the assessment of relative changes in the element contents (semi-quantitative EDS data) for each biomass as a function of the final pyrolysis temperature. We adopted the definition of "element enrichment" as the elemental difference between the final temperature of 900 °C (1000 °C for digested swine manure) and the original feedstock.

Enrichment in C was significant for endocarp casing (50.2%) and Candeia tree (34.3%), while the remaining statistically significant biochars tended toward C depletion. Coconut fiber showed C enrichment, but it was not sustained at 900 °C. In general, the proportional C enrichment for those biomasses can be associated with their relative lower ash content (Table 3).

All biochars showed N depletion, approximately -30% to -100%. Alternatively, the most significant P enrichment in biochar, 834%, was verified to epicarp casing, from 0.2% in the original feedstock to 2.3% in the 900 °C biochar. P-enrichment in the biochar from digested swine manure was 490%, from 1% to 6% in the 1000 °C biochar.

Changes in K reveal an enrichment trend above 500 °C for coconut fiber (903%), from 0.8% to 7.6%; epicarp casing (602%), from 2.72% to 19.1%; and endocarp casing (250%), from 1.1% to 3.8 %. K in living aquatic mats did not change significantly (Table 2), despite the high K content (Table 1). The K depletion in the digested swine manure

could have been due to volatilization at high temperatures (Keown *et al.* 2005), despite the high K content.

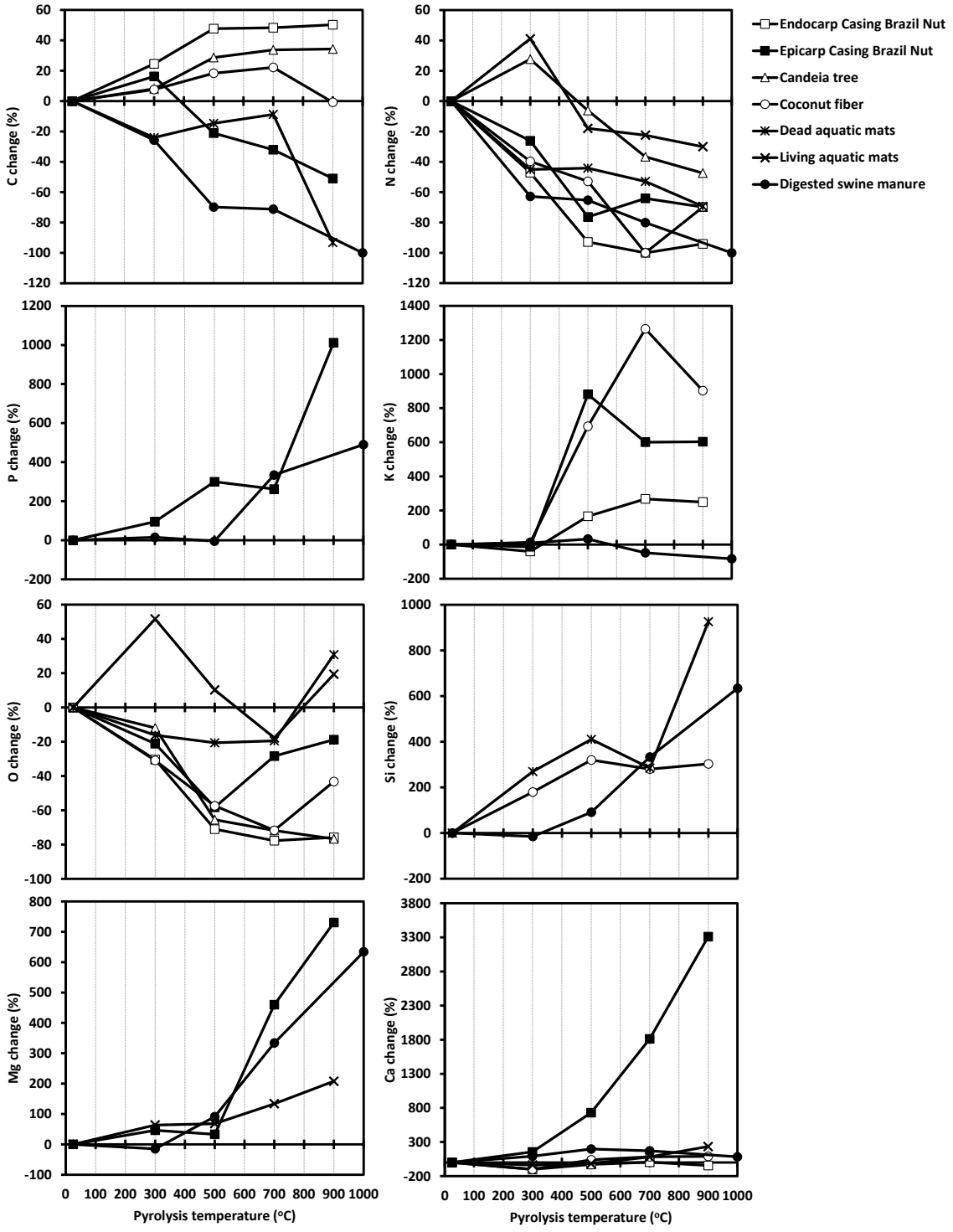

Fig. 3. Relative enrichment or depletion in C, N, P, K, O, Si, Mg, and Ca contents as a function of the initial (original) content and final pyrolysis temperatures for feedstocks with statistical significance shown in Table 2.

The O content decreased with increasing final pyrolysis temperature, except for living and dead aquatic mats. O-enriched biochars can be associated with high ash and mineral oxide particle contents (Table 3) *e.g.* silicates. Greater O depletion was verified for endocarp casing, Candeia tree, and coconut fiber. This is possibly due to the thermal decomposition of oxygen in carbohydrates of holocellulose and lignin.

Table 3. Proximate Analysis and Temperature Ranges at Maximum Mass Change and Methane Formation for the Biomass Feedstocks

	Holocellulose	Lignin	Moisture	Ashes	Volatile matter	Fixed carbon	Temp. @ max mass change	Temp. @ max CH_4 change
	wt.%						°C	
Endocarp casing Brazil nut	64.0[a]	31.9[a]	8.5	0.8	40.2	59.1	300 - 350	250 - 350
Epicarp casing Brazil nut	57.6[a]	37.7[a]	12.6	6.3	48.8	44.9	400 - 500	300 - 450
Candeia tree	53.1[a]	35.9[a]	6.5	0.49	39.2	60.3	300 - 350	250 - 350
Coconut fiber	42.7[a]	55.6[a]	8.5	5.41	44.8	49.8	250 - 350	250 - 350
Dead aquatic mats	50.3	16.7	5.6	42.2	31.9	25.9	300 - 400	250 - 350
Living aquatic mats	55.3	5.12	6.9	18.6	40.2	41.2	250 - 350	300 - 450
Digested swine manure	ND	ND	90.4	29.5	61.2	9.29	400 - 500	300 - 450

[a]Maia (2013)

(ND-not determined)

Significant Si enrichment was noted for digested swine manure, coconut fiber, and dead aquatic mats, while significant Mg enrichment was noted for epicarp casing, digested swine manure, and living aquatic mats (Table 2 and Fig. 3). Digested swine manure feedstock showed the greatest Mg content (Table 1) and a pronounced Mg enrichment of about 634%. In particular, the digested swine manure biochar contained a significant amount of struvite crystals ($NH_4MgPO_4 \cdot 6H_2O$), a slow release fertilizer (Rahman *et al.* 2014), as evidenced by SEM/EDS and FTIR analysis (Bergier *et al.* 2013) and by the elevated pH of approximately 8.5 of the biodigester effluent lagoon (unpublished data). Ca enrichment was also verified, particularly for epicarp casing (3312%), increasing from 0.2% in the feedstock to 7.2% in the 900 °C biochar (Fig. 3).

Thermal Decomposition and Methane Formation Curves

Curves in Fig. 4 indicate mass losses associated with thermal mass loss at 350 °C, as suggested by Zhao *et al.* (2013). The first mass loss stage, up to 150 °C, is an endothermic process related to water loss by sample drying, which was extended to 250 °C for the high-humidity digested swine manure sample (Fig. 4, Table 3). At 250 °C, a second mass loss stage appeared, corresponding to the decomposition of hemicellulose and cellulose structures (Pyrolysis I in Fig. 4). These exothermic events (DTA data in Fig. 4) took place simultaneously in all samples and had maximum mass loss rates between 250 and 350 °C. A third exothermic mass loss stage (Pyrolysis II in Fig. 4) was associated with

lignin thermal decomposition, with maximum mass loss in the range of 420 to 470 °C. Thermal mass loss of digested swine manure presented a pronounced peak at approximately 500 °C, likely related to complex organic compounds as fulvic acids produced by anaerobic processes (Bergier *et al.* 2013).

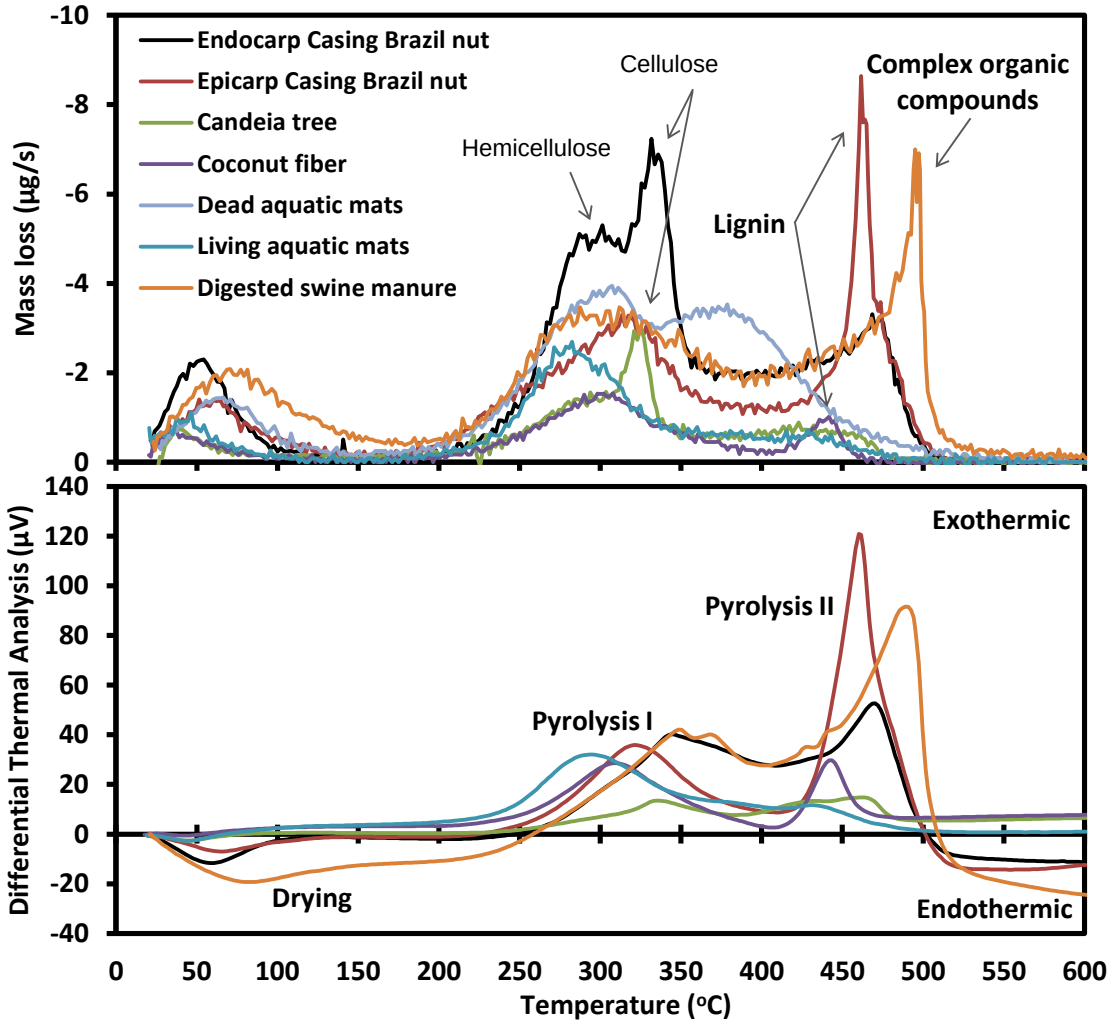

Fig. 4. Biomass thermal mass loss analysis by TG and DTA (DTA for dead aquatic mats was not obtained)

For the digested swine manure, the Pyrolysis I phase might be associated with the presence of functionalized structures with hydroxyl, carboxyl, and amide groups, and phosphorus and sulfur molecules (Bergier *et al.* 2013). The maximum mass loss rate for Pyrolysis I and II (Fig. 4) was usually near 250 to 350 °C and 400 to 500 °C, respectively.

Brazil nut endocarp casing and Candeia tree showed comparable thermal behavior, especially with respect to the Pyrolysis I phase (Fig. 4). The same was true for coconut fiber and Candeia tree. The latter showed a well-defined peak of cellulose and the former a well-defined peak of lignin, consistent with the proximate analysis (Table 3). Concerning the epicarp and endocarp casing of the Brazil nut, the former showed greater mass loss associated with lignin and the latter higher mass loss linked to hemicellulose and cellulose (Fig. 4 and Table 3).

Changes in methane formation during ESEM hot-stage pyrolysis are shown in Fig. 5. The two upper plots show the methane production (left-sided) and methane change (right-sided) for endocarp casing of the Brazil nut and Candeia tree. The middle plots illustrate methane production and change for coconut fiber, dead aquatic mats, and epicarp casing of the Brazil nut, whereas the lower plots show methane production and change for living aquatic mats and digested swine manure.

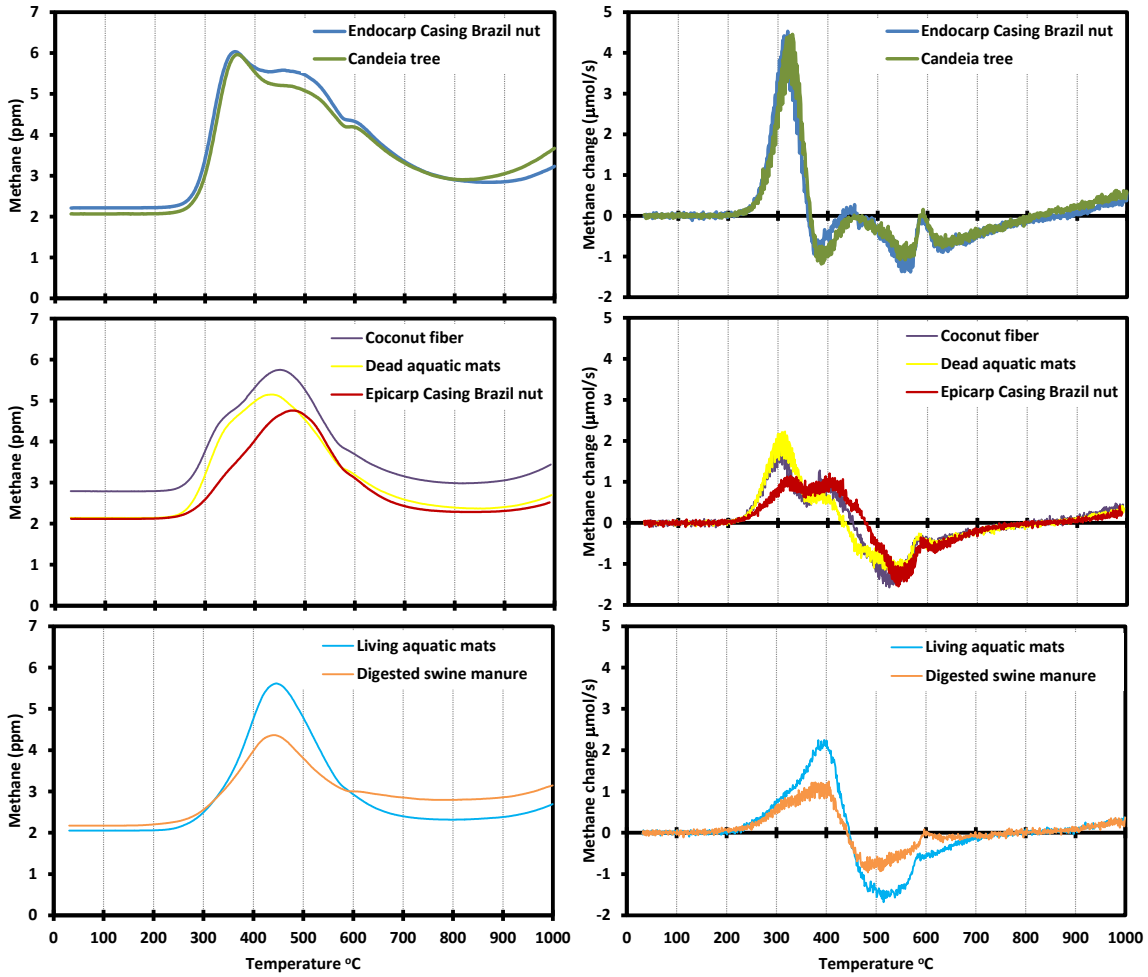

Fig. 5. Evolution of methane partial pressure (left side) and the according methane rate of change (right side) as a function of the hot-stage temperature increase in ESEM mode for each biomass. A common methane peak at around 600 °C (close to aluminum meting point) is likely associated with initial stages of aluminum cover melting (see https://youtu.be/aj1CerO6_Hc) allowing the release of retained gases produced early.

A clear feature is the pronounced CH_4 production corresponding to decomposition of volatile matter between 300 and 350 °C (Pyrolysis I phase in Fig. 4) and above 800 °C, which is likely associated with char and tar gasifications. The peak mass loss of lignin around 460 °C can also be noted in methane production curves (Fig. 5) for endocarp casing of the Brazil nut and Candeia tree. Alternatively, for the remaining biomass resources, methane formation rate increased at about 400 °C, which may be associated with their relatively higher ash content (Table 3) and the ongoing thermal degradation of the already charred materials.

CONCLUSIONS

The hot-stage EDS/ESEM/TDL technique is a relatively easily applied technique for low-vacuum biomass pyrolysis studies that provides very useful information allied with TG/DTA data. In this study, it was possible to verify that, as final temperature increases, N generally decreased by 30 to 100%, C increased by 20 to 50% for biomass rich in lignocellulose, and P, Mg and Ca increased for ash-rich biomass. Coconut fiber biochar is a good source of K. Methane formation also allows discriminating structural composition, providing fingerprints of each biomass. Biomass with low ashes and high lignin contents peaks CH_4 production at 330 and 460 °C, whereas those biomasses with high ashes and low lignin peaks CH_4 production at 330 and/or 400 °C. The final temperature of pyrolysis and the nature of the biomass feedstock can be combined for tailoring specific characteristics of the produced biochars such as the chemical element distribution.

ACKNOWLEDGMENTS

This research was partially supported by MCTI/CNPq, Grant 403161/2013-4.

REFERENCES CITED

Bergier, I., Vinhal-Freitas, I., and Guiotoku, M. (2013). "Low vacuum thermochemical conversion of anaerobically digested swine solids," *Chemosphere* 92, 714-720. DOI: 10.1016/j.chemosphere.2013.03.017

Bolan, N. S., Kunhikrishnan, A., Choppala, G. K., Thangarajan, R., and Chung, J. W. (2012). "Stabilization of carbon in composts and biochars in relation to carbon sequestration and soil fertility," *Science of the Total Environment* 424, 264-270. DOI: 10.1016/j.scitotenv.2012.02.061

Cantrell, K. B., Hunt, P. G., Uchimiya, M., Novak, J. M., and Ro, K. S. (2012). "Impact of pyrolysis temperature and manure source on physicochemical characteristics of biochar," *Bioresource Technology* 107, 419-428. DOI: 10.1016/j.biortech.2011.11.084

Case, S. D. C., McNamara, N. P., Reay, D. S., and Whitaker, J. (2012). "The effect of biochar addition on N_2O and CO_2 emissions from a sandy loam soil - The role of soil aeration," *Soil Biology and Biochemistry* 51, 125-134. DOI: 10.1016/j.soilbio.2012.03.017

Castro, W. J. P., Vianna, E. V., Salis, S. M., Galvani, F., and Bergier, I. (2010). *Composição Florística e Fauna Associada das Ilhas Flutuantes Livres, Rio Paraguai, Corumbá, MS*, V Simpósio sobre Recursos Naturais e Socioeconômicos do Pantanal, Corumbá. DOI: 10.13140/RG.2.1.3144.6883

Cayuela, M. L., van Zwieten, L., Singh, B. P., Jeffery, S., Roig, A., and Sánchez-Monedero, M. A. (2014). "Biochar's role in mitigating soil nitrous oxide emissions: A review and meta-analysis," *Agriculture, Ecosystems & Environment* 191, 5-16. DOI: 10.1016/j.agee.2013.10.009

Enders, A., Hanley, K., Whitman, T., Joseph, S., and Lehmann, J. (2012). "Characterization of biochars to evaluate recalcitrance and agronomic performance," *Bioresource Technology* 114, 644-653. DOI: 10.1016/j.biortech.2012.03.022

Gurwick, N. P., Moore, L. A., Kelly, C., and Elias, P. (2013). "A systematic review of biochar research, with a focus on its stability in situ and its promise as a climate mitigation strategy," *PLoS ONE* 8, e75932. DOI 10.1371/journal.pone.0075932

Keown, D. M., Favas, G., Hayashi, J., and Li, C.-Z. (2005) "Volatilisation of alkali and alkaline earth metallic species during the pyrolysis of biomass: differences between sugar cane bagasse and cane trash," *Bioresource Technology* 96, 1570-1577. DOI: 10.1016/j.biortech.2004.12.014

Lehmann, J., Rillig, M. C., Thies, J., Masiello, C. A., Hockaday, W. C., and Crowley, D. (2011). "Biochar effects on soil biota - A review," *Soil Biology and Biochemistry* 43(9), 1812-1836. DOI: 10.1016/j.soilbio.2011.04.022

Lima, R. M., and Maia, C. M. F. (2011). "*Potencial do resíduo da candeia (Eremanthus erythropappus) para a produção de biocarvão*," X Evento de Iniciação Científica da Embrapa Florestas, Colombo.

Liu, X.-Y., Qu, J.-J., Li, L.-Q., Zhang, A.-F., Jufeng, Z., Zheng, J.-W., and Pan, G.-X. (2012). "Can biochar amendment be an ecological engineering technology to depress N_2O emission in rice paddies? - A cross site field experiment from South China," *Ecological Engineering* 42, 168-173. DOI: 10.1016/j.ecoleng.2012.01.016

Maia, C. M. F. (2013). "*Produção de biocarvões por pirólise lenta: Potencial agrícola e ambiental*," X Encontro Brasileiro de Substâncias Húmicas, 2013, Santo Antônio de Goiás, Brasília.

Malik, A. (2007). "Environmental challenge *vis a vis* opportunity: The case of water hyacinth," *Environment International* 33(1), 122-138. DOI: 10.1016/j.envint.2006.08.004

Mukherjee, A. and Zimmerman, A. R. (2013). "Organic carbon and nutrient release from a range of laboratory-produced biochars and biochar–soil mixtures," *Geoderma* 193/194, 122-130. DOI: 10.1016/j.geoderma.2012.10.002

Mukome, F. N. D., J., S. and Parik, S. J. (2013). "The effects of walnut shell and wood feedstock biochar amendments on greenhouse gas emissions from a fertile soil," *Geoderma* 200/201, 90-98. DOI: 10.1016/j.geoderma.2013.02.004

Nelissen, V., Saha, B. K., Ruysschaert, G., and Boeckx, P. (2014). "Effect of different biochar and fertilizer types on N_2O and NO emissions," *Soil Biology and Biochemistry* 70, 244-255. DOI: 10.1016/j.soilbio.2013.12.026

Novotny, E. H., Hayes, M. H. B., Madari, B. E., Bonagamba, T. J., Azevedo, E. R., Souza, A. A., Song, G., Nogueira, C. M., and Mangrich, A. S. (2009). "Lessons from the Terra Preta de Índios of the Amazon region for the utilisation of charcoal for soil amendment," *Journal of the Brazilian Chemistry Society* 20(6), 1003-1010. DOI: 10.1590/S0103-50532009000600002

Paiva, P. M. V., Bergier, I., Novotny, E., and Maia, C. M. F. (2013). "*Relação entre temperatura de pirólise e a porosidade do mesocarpo de frutos da Castanheira-do-Brasil*," X EBSH - Encontro Brasileiro de Substâncias Húmicas, Santo Antônio de Goiás, GO. DOI: 10.13140/2.1.1024.0965

Rahman, M. M., Salleh, M. A. M., Rashid, U., Ahsan, A., Hossain, M. M., and Ra, C. S. (2014). "Production of slow release crystal fertilizer from wastewaters through struvite crystallization – A review," *Arabian Journal of Chemistry* 7, 139-155. DOI: 10.1016/j.arabjc.2013.10.007

Rajkovich, S., Enders, A., Hanley, K., Hyland, C., Zimmerman, A. R., and Lehmann, J. (2012). "Corn growth and nitrogen nutrition after additions of biochars with varying

properties to a temperate soil," *Biology and Fertility of Soils* 48, 271-284. DOI: 10.1007/s00374-011-0624-7

Spokas, K. A., Cantrell, K. B., Novak, J. M., Archer, D. W., Ippolito, J. A., Collins, H. P., Boateng, A. A., Lima, I. M., Lamb, M. C., McAloon, A. J., *et al.* (2012). "Biochar: A synthesis of its agronomic impact beyond carbon sequestration," *Journal of Environmental Quality* 41, 973-989. DOI: 10.2134/jeq2011.0069

Suddick, E. C. and Six, J. (2013). "An estimation of annual nitrous oxide emissions and soil quality following the amendment of high temperature walnut shell biochar and compost to a small scale vegetable crop rotation," *Science of the Total Environment* 465, 298-307. DOI: 10.1016/j.scitotenv.2013.01.094

Troy, S. M., Lawlor, P. G., Flynn, C. J. O., and Healy, M. G. (2013). "Impact of biochar addition to soil on greenhouse gas emissions following pig manure application," *Soil Biology and Biochemistry* 60, 173-181. DOI: 10.1016/j.soilbio.2013.01.019

Uchimiya, M., Ohnob, O., and Hea, Z. (2013). "Pyrolysis temperature-dependent release of dissolved organic carbon from plant, manure, and biorefinery wastes," *Journal of Analytical and Applied Pyrolysis* 104, 84-94. DOI: 10.1016/j.jaap.2013.09.003

Yoo, G., and Kang, H. (2012). "Effects of biochar addition on greenhouse gas emissions and microbial responses in a short-term laboratory experiment," *Journal of Environmental Quality* 41, 1193-1202. DOI: 10.2134/jeq2011.0157

Zhang, A., Bian, R., Hussain, Q., Li, L., Pan, G., Zheng, J., Zhang, X., and Zheng, J. (2013). "Change in net global warming potential of a rice–wheat cropping system with biochar soil amendment in a rice paddy from China," *Agriculture, Ecosystems and Environment* 173, 37-45. DOI: 10.1016/j.agee.2013.04.001

Zhao, L., Cao, X., Masek, O., and Zimmerman, A. (2013). "Heterogeneity of biochar properties as a function of feedstock sources and production temperatures," *Journal of Hazardous Materials* 256/257, 1-9. DOI: 10.1016/j.jhazmat.2013.04.015

Article submitted: July 13, 2015; Peer review completed: September 12, 2015; Revised version received: September 13, 2015; Accepted: September 14, 2015; Published: September 24, 2015.
DOI: 10.15376/biores.10.4.7604-7617